On the use of kurtosis control methods in shaker testing for fatigue damage

On the Use of Kurtosis Control Methods in Shaker Testing for Fatigue Damage

A. Steinwolf[1], B. Cornelis[2], B. Peeters[2], H. Van der Auweraer[2], M. Troncossi[3], A. Rivola[3]

[1]AST Consulting Ltd, 14A Croydon Road, New Lynn, Auckland, 0600, New Zealand;
e-mail: alexander.steinwolf@gmail.com
[2]Siemens Industry Software NV, Interleuvenlaan 68, Leuven, 3001, Belgium;
[3]Department of Engineering for Industry, University of Bologna, via Fontanelle 40, Forlì, 47121, Italy.

Abstract: Random vibration testing with increased kurtosis introduces high peaks into shaker drive signals to simulate land vehicle vibration more accurately and, also, to shorten the required test time. Two methods of controlling kurtosis by phase manipulation in the inverse fast Fourier transform were implemented, tested, and compared. The first method generates high-kurtosis excitations with a gradual, smooth pattern of peak heights from low to high and the second method produces isolated high peaks with intervals of stable background vibration between them. When applying kurtosis increase for accelerated fatigue damage testing, the kurtosis control method must be able to pass high kurtosis values from the generated shaker table vibration into the stress response of the unit under test. However, this is not always the case and only one of the considered methods was capable of doing so. In the paper the fatigue damage spectrum model was used for evaluation of time-to-failure. An experimental study was carried out using operational vibration measured in a car. Shaker testing of cantilever specimens was performed for Gaussian, non-Gaussian, and accelerated non-Gaussian excitations.

Keywords: shaker testing; kurtosis; IFFT phases; fatigue damage spectrum, accelerated lifetime testing.

Nomenclature

A_n	= amplitude of n-th harmonic in the excitation signal
b	= Wohler curve slope
f	= frequency
Δf	= frequency increment of the discretized PSD
i	= iteration number in the outer-loop iterative procedure
j	= iteration number in the inner-loop iterative procedure
K	= kurtosis value of an excitation or system response signal
K_i^{dr}	= kurtosis value of the drive signal on the previous outer-loop iteration
K_{i+1}^{dr}	= kurtosis value of the drive signal on the next outer-loop iteration
K_{spec}	= kurtosis value in the test specification prescribed for shaker table vibration
K_i^{vib}	= kurtosis value of the vibration signal measured on the shaker table
K_j^{p}	= kurtosis value after the polynomial transformation on the j-th inner-loop iteration
K_1^{tfs}	= kurtosis value after the time-frequency domain swapping on the j-th inner-loop iteration
L	= number of instantaneous values of signal $x(m\Delta t)$ on the time interval where the excitation or system response signal is observed
N	= number of harmonics in the excitation multi-frequency signal
$Q(x)$	= Gaussian-to-non-Gaussian polynomial transformation function
$S(f)$	= power spectral density (PSD) of the excitation signal
$S(n\Delta f)$	= discretized PSD of the excitation signal
$S_i^{dr}(n\Delta f)$	= discretized PSD of the drive signal on the previous outer-loop iteration
$S_{i+1}^{dr}(n\Delta f)$	= discretized PSD of the drive signal on the next outer-loop iteration
$S_{spec}(n\Delta f)$	= discretized PSD of the test specification prescribed for shaker table vibration
$S_i^{vib}(n\Delta f)$	= discretized PSD of the vibration signal measured on the shaker table

T	= length of time interval on which excitation or system response signal is observed
t	= time
Δt	= time step of signal discretization
$x(t)$	= time history of an excitation or system response signal
$x(m\Delta t)$	= instantaneous values of an excitation or system response signal after discretization
$y(t)$	= non-Gaussian signal obtained as an output of the polynomial transformation
α	= coefficient to ensure the correct root-mean-square (RMS) value of the polynomial transformation output signal
β	= coefficient to ensure the required kurtosis of the polynomial transformation output
$F(\omega)$	= frequency response function of the single-degree-of-freedom (SDOF) system of the tested cantilever specimen
φ_n	= phase of n-th harmonic in the excitation signal
σ	= RMS value of an excitation or system response signal
σ_y	= RMS value of the polynomial transformation output signal
ω_p	= frequency corresponding to the position of the resonance peak
ω_1 and ω_2	= frequencies corresponding to positions where the FRF amplitudes $F(\omega_1)$ and $F(\omega_2)$ squared become twice less than the peak amplitude $F(\omega_p)$ squared
ω_R	= resonance frequency of the SDOF system in the fatigue damage spectrum (FDS) model
ζ	= damping factor of the SDOF system in the FDS model

1. Introduction

In automotive and aerospace engineering, vehicle components are exposed to dynamic loads that may induce failures. These loads are influenced by many unpredictable factors and, therefore, become random excitation signals. To validate whether the components will remain unbroken and functioning during the service life, they are subjected to vibration tests on electrodynamic shakers [1-4]. It is now established practice to develop qualification test specifications based on the actual environmental conditions where the vehicle is deployed. The objective is to have damage equivalence between the in-service excitation data and the qualification test profile, meaning that the fatigue damage accumulated over the operational lifetime of the vehicle component has to be recreated in the in-house qualification test. This method uses a concept of the fatigue damage spectrum (FDS) [3].

When performing qualification tests in the laboratory, it is of interest not only to simulate in-service vibrations but also to shorten the testing time, i.e. to accelerate obtaining the required results by reducing the total test duration in a controlled manner [4]. The time-to-failure in the shaker testing has to be decreased while maintaining the accumulated damage equivalence between the operational data and the qualification test. Currently, when designing an accelerated lifetime test [4], the shaker random excitation is specified by the power spectral density (PSD) and the fatigue damage model is described by the Wohler curve (S-N curve). In so doing a simple power upscaling can be implemented. To inflict the same damage in shorter test duration, the overall PSD level has to be increased proportionally [4]. However, there are several caveats when using this approach [3-5].

If the PSD level is increased too much, the breakdown of the tested component may no longer be due to fatigue, which was the cause of failure in operation. Also, in the more severe testing, the unit under test may start behaving as nonlinear dynamic system whereas a linear system response is assumed in the FDS model. Another danger is that, for materials with an endurance limit, small cycles, which were non-damaging for the operational PSD level, may be scaled over the endurance limit so that the damage accumulated in testing becomes higher than expected. Finally, some error may be introduced because the evaluated slope of the Wohler curve is sensitive to the load level which in testing becomes higher than in operation. For all these reasons, the standards suggest that the test exaggeration factor, which is the ratio of the test PSD level to the operational PSD level, should be kept to minimum [1].

Modern shaker control systems can generate random excitations according to the prescribed PSD profile by implementing the inverse fast Fourier transform (IFFT). After being used for vibration testing of vehicle components for several decades, this procedure has recently been supplemented with simultaneous kurtosis control. Kurtosis is a basic characteristic of probability distributions and it is widely used by statisticians. If $x(t)$ is a time history of a stationary ergodic random signal observed in the time interval $[0,T]$ then its kurtosis value is determined according to the following equation

$$K = \frac{1}{\sigma^4 T}\int_0^T [x(t)]^4 dt \tag{1}$$

that is the theoretical definition of kurtosis. Alternatively, if a time history sample is prescribed by discrete instantaneous values $x(m\Delta t)$ of the signal under consideration, where $m=1,2,\ldots, L$ and $L=T/\Delta t$, then the kurtosis estimate can be calculated

$$K = \frac{\frac{1}{L}\sum_{m=1}^{L}[x(m\Delta t)]^4}{\left\{\frac{1}{L}\sum_{m=1}^{L}[x(m\Delta t)]^2\right\}^2} \tag{2}$$

by replacing integration in Eq (1) with summation and also by doing the same for the root-mean-square (RMS) value σ in the denominator of Eq (1).

For a Gaussian signal the kurtosis is equal to 3. If it is made higher than that, non-Gaussian severe peaks will be present in the signal. In shaker testing this was necessary to overcome inconsistency between Gaussian random signals of shaker excitations generated by the traditional PSD control and operational vibrations of land vehicles that appear to have time history peaks much higher than those predicted by the Gaussian model [6-11]. Nowadays, the same methodology of additional kurtosis control is considered for another purpose of deliberately increasing severity of shaker excitations in order to carry out fatigue durability testing in a shorter time [12].

Fatigue damage imposed on the unit under test would be accumulated faster by applying excitations with amplified kurtosis because generating higher time history peaks means having larger cycle amplitudes. This paper explores a way of implementing the kurtosis increase approach without any magnification of the excitation PSD. Exercising accelerated testing with the PSD specification preserved would allow to avoid the aforementioned caveats of reducing test duration by scaling up the PSD observed in operational conditions. However, this is not a trivial task because the response of a lightly-damped linear system (that is what the breaking component is supposed to be) will be closer to a Gaussian random signal than the non-Gaussian excitation applied by the shaker. It has been verified numerically [13] and experimentally [14] that, even if the shaker table vibration possesses a high kurtosis, it may not be sufficient to achieve higher enough kurtosis for the stress random signal in the elastic element where the structural fatigue occurs.

2. Qualification Testing and Fatigue Damage Spectrum

The main objective of qualification testing is to replicate the effect of operational environments on the unit under test in terms of the damage accumulated due to occurrence of structural fatigue [2]. If the cause of product failure is high-cycle fatigue and dangerous stress levels arise because a system resonance is excited by the excitation applied then the fatigue damage spectrum can be used to quantify the damage potential of different excitations. A typical situation for doing so is when the unit under test (e.g. electronic device in a vehicle) is a complex system for which it is hard to identify actual resonances of all system elements. Instead, it is supposed that a resonance can be at any frequency of the excitation frequency band and a linear single-degree-of-freedom (SDOF) model is implemented to estimate the dynamic response of these hypothetical elements.

In order to obtain the FDS value for certain resonance frequency ω_R, first a calculation is made where a realistic or shaker-generated vibrational excitation is applied to the base of SDOF system with an assumed damping factor ζ [2,3]. This results in a relative displacement response signal which is subsequently processed by a rain-flow cycle counting algorithm because it is supposed that the stress in the SDOF system elastic part is proportional to the relative displacement. Then, the Wohler curve with an assumed slope coefficient b and the Miner rule of linear damage accumulation are employed to predict what fraction of the full damage corresponding to fatigue failure has been accumulated during the total length of the excitation signal applied. The ratio of the fractions of the full damage determined for the excitation generated in shaker testing and the excitation observed in operation constitutes relative damage estimated for these two excitations.

The shaker excitation in this methodology is meant to be either a test profile targeting the same damage as in operation or a deliberately intensified excitation profile to accelerate the in-house testing and get the result of product validation faster. The notion of fatigue damage spectrum implies that the described algorithm is applied for a number of assumed resonance frequencies ω_R one by one and the damage result is presented as a function of ω_R, i.e. spectrum.

However, this paper considers only one point of the FDS curve to focus on the new idea of controlling the fatigue damage inflicted by shaker system without introducing any changes into the excitation PSD to overcome the above-mentioned problems associated with the PSD level increase. From the practical point of view, a method of controlling a single FDS point will be useful for the case of testing a vehicle component with its resonance frequency known from experimental measurements when, for instance, fatigue durability of a fixture connecting this component to the main body of the vehicle appears to be unsatisfactory and possible design improvements need to be tested.

As discussed in the Introduction, the shaker-generated excitation can be made more severe by increasing its kurtosis. Possible solutions for doing so are discussed in the next section of the paper. Two methods of controlling kurtosis by manipulation of the IFFT phases were considered in relation to the specifics and requirements of qualification testing for fatigue durability. These methods were implemented in computer algorithms, for which a comprehensive and thorough verification programme described later in the paper was carried out. Then, an example of in-service vibration measured in a car was analyzed and an experiment of shaker testing of cantilever specimens was performed for Gaussian, non-Gaussian, and accelerated non-Gaussian excitations.

3. Kurtosis Control Methods.

Shaker controllers for random vibration testing use the IFFT procedure to derive excitation signals from the prescribed PSD profile. It means that the shaker is driven by a multi-frequency signal

$$x(t) = \sum_{n=1}^{N} A_n \cos(2\pi n \Delta f t + \varphi_n) \tag{3}$$

with a large number of harmonics N. The amplitudes of the harmonics are determined

$$A_n = \sqrt{2\Delta f S(n\Delta f)} \tag{4}$$

to match the given PSD shape $S(f)$ that is discretized with the frequency increment Δf. The phases φ_n can be defined as samples of a random variable uniformly distributed in the range from $-\pi$ to π radians. If a new set of phase values is used in each subsequent data block generated according to Eq (3) then such an excitation of any duration will look like a random signal which never repeats itself.

The discrete Fourier transform model by Eqs (3) and (4) is convenient for digital shaker controllers because it allows easy correction of the drive signal PSD shape using the results of analysis of the vibration feedback signal from the shaker table where a unit under test is affixed. A closed-loop iteration procedure should be arranged to control the PSD of the generated vibration because the height of a

certain spectrum line $S_i^{vib}(n\Delta f)$ located at the frequency $f=n\Delta f$ in the shaker table vibration PSD on the i-th iteration may become more (or less) than what it should be according to the test specification $S_{spec}(n\Delta f)$ at this frequency. To compensate for the difference between $S_i^{vib}(n\Delta f)$ and $S_{spec}(n\Delta f)$, the height of the same spectrum line $S_{i+1}^{dr}(n\Delta f)$ in the drive signal PSD on the next (i+1)-th iteration should be decreased (or increased) compared to what it was on the previous iteration $S_i^{dr}(n\Delta f)$.

Mathematically the above is expressed as

$$S_{i+1}^{dr}(n\Delta f) = S_i^{dr}(n\Delta f)\frac{S_{spec}(n\Delta f)}{S_i^{vib}(n\Delta f)}, \qquad n = 1,2,3,\ldots,N. \tag{5}$$

Equation (5) repeated for each of N spectrum lines gives the full PSD of the drive signal for the next iteration. Then all discrete spectrum values $S_{i+1}^{dr}(n\Delta f)$ obtained are substituted into Eq (4) for harmonics amplitudes and a new drive signal time history is generated according to Eq (3). Such iterations are continued until the spectrum $S_i^{vib}(n\Delta f)$ of the shaker table vibration feedback signal is close enough to the specified target profile $S_{spec}(n\Delta f)$ and, thus, the PSD simulation requirement is fulfilled.

This is how it had been before additional kurtosis control by phase manipulation [7,10] was introduced. Now, the phase angles φ_n have become non-Gaussian simulation variables instead of being random as in common shaker controllers with the traditional IFFT generation procedure. It is possible to control kurtosis and achieve the specified high kurtosis value K_{spec} in the same iterative manner as for the PSD. If the kurtosis value K_i^{dr} of drive signal is increased, the kurtosis K_i^{vib} of the shaker table vibration feedback will follow or vice versa if the kurtosis decrease is needed. Hence the kurtosis can be adjusted similarly to how it was discussed above for the height of a PSD line

$$K_{i+1}^{dr} = K_i^{dr}\frac{K_{spec}}{K_i^{vib}} \tag{6}$$

with only one such correction for the entire random signal, not N corrections for every spectrum line.

When the kurtosis value for the next iteration of shaker control procedure is determined by Eq (6), a big question arises about how the IFFT phases should be manipulated to actually generate the shaker drive signal (3) such that it has the required kurtosis value K_{i+1}^{dr}. It is discussed below how this can be done simultaneously with maintaining the necessary PSD shape $S_{i+1}^{dr}(n\Delta f)$ by proper choice of the IFFT amplitudes A_n.

3.1 Method 1: Polynomial Transformation with Time-Frequency Domain Swapping

This method is based on a well-known approach [8,15], which is to generate a Gaussian time history with the given PSD first and, then, to modify it into a non-Gaussian signal with the help of polynomial transformation $y=Q(x)$. For kurtosis increase such transformation is accomplished by a combination of two terms: linear and cubic

$$y(t) = \alpha[x(t) + \beta x^3(t)] \tag{7}$$

In so doing, those instantaneous values of the initial Gaussian signal $x(t)$ that are larger than its RMS value will be stretched towards producing higher peaks. As a result, the transformed signal $y(t)$ acquires higher kurtosis but the cubic function (7) applied to the Gaussian input also affects the PSD. This is an unwanted disturbance of the test specification because the PSD of the transformed signal with increased kurtosis will no longer correspond exactly to the given PSD profile.

Such a situation is unacceptable since the PSD simulation remains a mandatory requirement that must be fulfilled in non-Gaussian random shaker testing. This difficulty discussed in the previous research [11,16] restricted the polynomial transformation method to being used only for mild non-Gaussian cases

because, the higher the required kurtosis is, the harder the PSD distortions are. However, if the polynomial transformation is combined with the time-frequency domain swapping algorithm [17,18], the PSD distortions can be avoided by introducing an inner-loop iterative procedure performed on every iteration of the outer-loop shaker control according to Eqs (5) and (6). These inner-loop iterations were carried out as follows.

After the basic polynomial transformation by cubic function (7) has been performed, a time history with the kurtosis value K_{i+1}^{dr} required for the next (i+1)-th iteration of the outer-loop shaker control will be obtained. However, it cannot be used as the shaker drive signal because its PSD is corrupted. Instead, it is suggested that this non-Gaussian time history is converted into the frequency domain by the FFT procedure. The phase spectrum obtained in this way is useful since it corresponds to the required high kurtosis value. However, the amplitude spectrum is now different from the required PSD $S_{i+1}^{dr}(n\Delta f)$ because of the frequency distortions introduced by the polynomial transformation.

The idea of the improved Gaussian-to-non-Gaussian transformation method is to discard the amplitude spectrum corrupted by polynomial transformation of the Gaussian signal and replace it with the amplitude spectrum of the exact $S_{i+1}^{dr}(n\Delta f)$ profile. Then, the IFFT procedure is applied to return to the time domain by combining the amplitudes of the required PSD with the phase spectrum corresponding to higher kurtosis. At the end of this first inner-loop iteration of the time-frequency domain swapping procedure, the time history obtained has a kurtosis value K_1^{tfs} lower than the kurtosis value K_1^{p} obtained initially by the polynomial transformation but higher than the Gaussian kurtosis K=3.

Thus, some progress has been achieved and this inner-loop iterative process can be continued by subjecting the initial Gaussian signal to polynomial transformation again but now with a new required kurtosis value K_2^{p} larger than the kurtosis $K_1^{p} = K_{i+1}^{dr}$ used to construct the corresponding polynomial transform function (7) on the first inner-loop iteration. Then, the FFT and IFFT conversions of the time-frequency domain swapping procedure described above are repeated and the next kurtosis value K_2^{tfs} of the new output signal with the corrected amplitude spectrum is obtained.

A critical question in the implementation of the described algorithm is how to prescribe the input kurtosis value K_{j+1}^{p} for the polynomial transform (7) on the next *(j+1)*-th iteration of the time-frequency domain swapping algorithm. To have iteration process of updating K_j^{p} values effective and to force the sequence of K_j^{tfs} values of generated output signals to converge to the kurtosis value K_{i+1}^{dr} of the shaker drive signal on the next outer-loop iteration, one needs to use properly the input K_j^{p} and output K_j^{tfs} kurtosis values from the previous *j*-th iteration of the inner-loop.

After testing several possible ways of calculating the kurtosis value K_{j+1}^{p} to be used as the target of polynomial transformation on the next time-frequency domain swapping iteration, the following equation, similar to Eq (6) of the outer-loop shaker control, was adopted

$$K_{j+1}^{p} = K_j^{p} \frac{K_{i+1}^{dr}}{K_j^{tfs}} . \tag{8}$$

When the kurtosis value K_{j+1}^{p} is found, the polynomial transform function (7) can be constructed by calculating the coefficient β either in terms of the Hermite polynomials [15] or strait by the expression of β via the required kurtosis value obtained from Eq (8)

$$\beta = \frac{-2 + \sqrt{6K_{j+1}^{p} - 14}}{3\left(14 - \sqrt{6K_{j+1}^{p} - 14}\right)}$$

as suggested in Ref [11]. The role of the coefficient α in Eq (7) is to ensure that, after β is determined, the necessary RMS value σ_y of the output signal *y(t)* is also achieved, simultaneously with the required kurtosis value. The equation for α is as follows

$$\alpha = \frac{\sigma_y}{\sqrt{1 + 6\beta + 15\beta^2}}$$

In the computer trials of the polynomial transformation algorithm it was found that the speed of non-Gaussian signal generation can be improved if the K_1^p value at the start of the time-frequency domain swapping iterations for the next data block is prescribed equal not to K_{i+1}^{dr} but to the last K_{j+1}^p value from the inner-loop iteration process for the previous data block.

3.2 Method 2: Analytical Solution for Phases Based on Kurtosis Equation

The time-frequency domain swapping, now used for generating non-Gaussian random excitations with increased kurtosis, is a numerical procedure. Each iteration of the algorithm described in the previous subsection consists of two FFT computations (direct and inverse) plus calculation of polynomial transformation. The necessity of all these computational processes may slow down shaker controller operation and, therefore, an analytical solution, which is supposed to be faster, would be preferable. Such a solution has previously been developed [11,19] and it is presented here as the second method of phase manipulation for controlling kurtosis of the IFFT-generated signal.

Distinct from the kurtosis estimation for a discretized random data sample by Eq (2), the kurtosis of a signal obtained by the IFFT generation can be derived from the theoretical definition by Eq (1) because, for the IFFT-generated pseudo-random multi-frequency signal, there is a formula representing the time history analytically by Eq (3), not just discrete numerical values *x(mΔt)* as for a data sample. This gives an opportunity to express the kurtosis via the amplitudes A_n and phases φ_n of the multi-frequency signal (3) and to use this expression for developing a method of manipulating the amplitudes and phases in order to control kurtosis additionally to the ordinary PSD control.

A closed-form equation expressing the kurtosis via the amplitudes A_n and phases φ_n of the IFFT-generated signal (3) has been obtained in the following form [10]

$$K = 3 - \frac{3\sum_{n=1}^{N} A_n^4}{2(\sum_{n=1}^{N} A_n^2)^2} + \frac{2}{(\sum_{n=1}^{N} A_n^2)^2}\left\{ 6 \sum_{\substack{j+k=m+n \\ j<k, m<n, m<j}} A_j A_k A_m A_n \cos(\varphi_j + \varphi_k - \varphi_m - \varphi_n) \right.$$
$$+ 6 \sum_{\substack{j+k+m=n \\ j<k<m}} A_j A_k A_m A_n \cos(\varphi_j + \varphi_k + \varphi_m - \varphi_n) + \sum_{j=3k} A_j A_k^3 \cos(\varphi_j - 3\varphi_k)$$
$$\left. + 3 \sum_{\substack{j=k+2m \\ k \neq m}} A_j A_k A_m^2 \cos(\varphi_j - \varphi_k - 2\varphi_m) + 3 \sum_{\substack{j+k=2m \\ j<k}} A_j A_k A_m^2 \cos(\varphi_j + \varphi_k - 2\varphi_m) \right\} \quad (9)$$

where special conditions must be met for the sums inside the curly brackets. The summation is performed only for those combinations of subscripts *j, k, m, n* that satisfy equalities and inequalities written under the summation symbols.

It is clear from this equation that the kurtosis can be changed by manipulating the phases while keeping the amplitudes fixed according to Eq (4) to preserve the specified PSD. When using Eq (9), there is no need in inner-loop iterations of kurtosis adjustment and the PSD corrections as with the time-frequency domain swapping. The phases increasing kurtosis can be found from Eq (9) without any attempts of actually generating time histories. The IFFT signal generation is performed only once, not many times, and multiple FFT procedures and polynomial transformations are avoided to save computation time.

If the phase angles φ_n are chosen in a random manner, as in the traditional Gaussian random testing, then the cosine functions in Eq (9) produce random values which are distributed in the interval from -1 to 1. These random values corresponding to many different subscript groups *j, k, m, n* compensate each other and bring the result of summation in all phase-dependent terms close to zero. Thus, for random phases, the phase-dependent terms do not take the kurtosis away from the Gaussian value of 3 introduced by the first term in Eq (9). However, this can be changed if the phase selection strategy is not simply a random choice.

If the argument of a cosine function in Eq (9) is changed to zero by virtue of one of the phases being expressed via the others [11] then this cosine function will produce not a random value but the value of 1. Consequently, the corresponding member of the summation is forced into its largest possible value. For example, for the first sum inside the curly brackets in Eq (9)

$$\sum_{\substack{j+k=m+n \\ j<k, m<n, m<j}} A_j A_k A_m A_n \cos(\varphi_j+\varphi_k-\varphi_m-\varphi_n),$$

such maximization of the cosine function output is achieved by making one of the phases, say φ_k, not random but calculated as $\varphi_k = \varphi_m + \varphi_n - \varphi_j$ via the other three phases that remain random.

In so doing, the largest value $A_j A_k A_m A_n$ is obtained for the corresponding member of the summation under consideration instead of some value between $-A_j A_k A_m A_n$ and $A_j A_k A_m A_n$ produced when all phases involved are random. If a similar phase selection is made not for one subscript group *j, k, m, n* but for many of them and also for other summation terms of Eq (9), this results in a tendency for kurtosis to increase. It is the essence of the kurtosis control procedure by the second phase selection method based on the analytical expression of kurtosis via the IFFT amplitudes and phases.

4. Verification and Performance Comparison of Two Procedures for Phase Selection.

The phase selection methods of increasing kurtosis described in the previous section were implemented in computer algorithms, for which a comprehensive and thorough testing programme was carried out. The first question that needed to be addressed was about the limits of kurtosis increase achievable by each of the two methods. To get an answer to this question for the time-frequency domain swapping method, the inner-loop iteration algorithm described above was tried with a wittingly high outer-loop kurtosis target value of K_{i+1}^{dr}=20. The results of this kind of algorithm verification, which was performed for the uniform PSD profiles, are shown in Fig. 1 in comparison with the dotted horizontal line representing the K_{i+1}^{dr} value.

The thick solid curves depict kurtosis values K_j^{tfs} achieved on inner-loop iterations of the time-frequency domain swapping process. The kurtosis results for different data blocks are separated from each other by thin vertical lines. When a time history consisting of several IFFT data blocks was generated by the method of polynomial transformation with time-frequency domain swapping, it appeared that the iteration process of kurtosis increase does not always reach the outer-loop target kurtosis value K_{i+1}^{dr} if it is high. As one can see in Fig. 1, the kurtosis values K_j^{tfs} obtained in iterations for a particular data block have maximum at certain level and, then, start decreasing, nevertheless the kurtosis values K_j^{p} prescribed for the polynomial transform (7) continued to grow.

a) Kurtosis results for wideband PSD profile with 1000 frequency lines
b) Kurtosis results for narrowband PSD profile with 100 frequency lines

Fig. 1. Time-frequency domain swapping iteration processes demonstrating maximum kurtosis values achieved for different IFFT data blocks

If the iteration process goes on, the kurtosis value eventually stabilizes at the level that is substantially lower than the aforementioned maximum kurtosis value achieved on earlier inner-loop iterations for the same data block. The latter should be taken into account when programming this algorithm into an automatic shaker controller. The software must restrict the number of time-frequency domain swapping iterations for one data block in order to be able to stop the iterative process when the output kurtosis values K_j^{tfs} stabilize and there is no hope anymore of achieving the outer-loop kurtosis target value K_{i+1}^{dr}.

However, simply to take the time history corresponding to the stabilized kurtosis value K_j^{tfs} as the generated drive signal will result in unnecessarily lower kurtosis. It is better to keep track of the K_j^{tfs} values on all inner-loop iterations and return to that particular iteration when the output kurtosis value was the largest. By repeating the polynomial transform (7) for the kurtosis value K_j^{p} corresponding to this largest K_j^{tfs} value and doing time-frequency swapping once more, the undershooting of the kurtosis target will be minimized by obtaining a signal with the best possible kurtosis value for the current initial Gaussian data block.

It was observed in testing of the algorithm of polynomial transformation with time-frequency domain swapping and can be seen in Fig. 1 that the maximum achievable kurtosis value fluctuates essentially depending on the state of the Gaussian IFFT data block subjected to the polynomial transform (7). This is because the highest peaks in the initial Gaussian data block still vary to certain extent and those Gaussian peaks, which are relatively higher than that in other data blocks, are easier to pull to non-Gaussian heights by the polynomial transformation. Further verification of this algorithm of phase manipulation revealed that the maximum achievable kurtosis value for narrowband PSD test specifications is lower on average than for the wideband spectra specifications.

In the example of generating 10 data blocks presented in Fig. 1,a, the required PSD profile was wideband with 1000 frequency lines in the shaker controller setup. In this case, the outer-loop kurtosis target value K_{i+1}^{dr}=20 was achieved for 2 data blocks, with the other 8 blocks having reduced kurtosis values between 8 and 17. For the narrowband PSD test specification with 100 frequency lines (Fig. 1,b), 9 of 10 data blocks generated with the help of the time-frequency domain swapping resulted in kurtosis values twice lower than the target of K_{i+1}^{dr} =20. This means that, kurtosis values of these data blocks fell short of some typical kurtosis specifications required in practice of environmental shaker testing.

A broader and more detailed picture is given by Figs. 2, 3, and 4 of what happens with success rates of achieving three realistic kurtosis specifications of K=6, K=9, and K=12 if the PSD frequency range is narrowed from 1000 to 500 and, then, to 100 frequency lines. Kurtosis values for different IFFT blocks are shown by points sitting on the horizontal line representing the target kurtosis value or positioned below it. Those kurtosis values, which are less than the kurtosis target, correspond to situations when the time-frequency swapping was stopped by the condition of the limiting number of iterations being reached (this number was set to 10). The kurtosis simulation success rates and total kurtosis K_t for the entire signal of 20 blocks are given in the figure captions. Both these values drop when the target kurtosis is increasing or the number of PSD frequency lines in the test profile is decreasing.

Having obtained all the above results for the method of polynomial transformation with time-frequency domain swapping, it was then necessary to perform similar testing of the method of analytical phase selection. The same three cases of wideband (1000 frequency lines), intermediate (500 lines), and narrowband (100 lines) PSD profiles were considered again for the typical kurtosis specifications of K=6, K=9, and K=12. The result of this was that all three kurtosis target values were achieved for every data block generated in all three cases of the wideband, narrowband, and intermediate excitations, making the kurtosis success rate equal to 100%.

a) K=6 in 100% of blocks, K_t=6 b) K=9 in 95% of blocks, K_t=8.9 c) K=12 in 60% of blocks, K_t=11

Fig. 2. Kurtosis simulation success rates by the method of polynomial transformation with time-frequency domain swapping for PSD profile with 1000 frequency lines.

a) K=6 in 100% of blocks, K_t=6 b) K=9 in 75% of blocks, K_t=8.5 c) K=12 in 35% of blocks, K_t=9.4

Fig. 3. Kurtosis simulation success rates by the method of polynomial transformation with time-frequency domain swapping for PSD profile with 500 frequency lines.

a) K=6 in 75% of blocks, K_t=5.6 b) K=9 in 40% of blocks, K_t=6.9 c) K=12 in 15% of blocks, K_t=7.3

Fig. 4. Kurtosis simulation success rates by the method of polynomial transformation with time-frequency domain swapping for PSD profile with 100 frequency lines.

Furthermore, by the method of analytical phase selection based on the kurtosis equation, kurtosis values higher than K=12 were also achieved. On the other hand, for the method of polynomial transformation with time-frequency domain swapping, the kurtosis success rate of 100% occurred only for the kurtosis value K=6 and not for K=9 and K=12. In the case of narrowband excitation, even the smallest kurtosis value of K=6 was not always possible.

Apart from the difference in achievable kurtosis values the two methods of non-Gaussian phase manipulation are also different in appearance of time histories even when the two compared signals have the same kurtosis. The method of polynomial transformation with time-frequency domain swapping generates signals (Fig. 5,a) with a gradual, smooth pattern of peak heights from low to high such as in random noise. On the other hand, the analytical phase selection based on the kurtosis equation produces isolated high peaks with intervals of stable background vibration between them (Fig. 5,b) such as if a vehicle encounters a distinctive irregularity on the road from time to time. Thus, it would be useful to have both these methods in shaker controller options for more flexibility of generating non-Gaussian random excitations of different kinds.

a) Polynomial transformation with time-frequency domain swapping

b) Analytical phase selection based on kurtosis equation

Fig. 5. Shaker excitation time histories generated by two different methods of kurtosis control.

Numerical verification of the polynomial transformation with time-frequency domain swapping algorithm has shown that its kurtosis simulation capabilities are limited to K=10 for wideband PSD profile and K=5 for narrowband one. This might be sufficient for successful environmental testing with simultaneous PSD and kurtosis control in the case of the unit under test being fixed to the shaker table rigidly. However, qualification testing with implementation of the FDS model, which is the subject of this paper, is of another kind because the unit under test is supposed to be a SDOF system with its elastic element being prone to fatigue failure. Therefore, performance of the kurtosis increase methods under consideration should have been evaluated specifically for such a situation.

5. Experimental Results

With the aim of experimentally verifying effects of the high-kurtosis excitation signals on real mechanical components, a number of tests were performed. A flat specimen of rectangular shape and rectangular cross section, 165 mm long, 25 mm wide, and 3 mm thick was designed for this purpose (Fig. 6). The specimen made of aluminium alloy 6082 was rigidly mounted with four screws on a stiff fixture in a cantilever configuration. It carried an additional mass of 1.8 kg close to its free end. The specimen's natural frequency corresponding to the first flexural mode shape was found to be at about 12 Hz.

Fig. 6. Experimental setup: the cantilever specimen mounted on the shaker.

The specimen was excited by imposing vertical vibratory motion to its base. This excitation was provided by a single-axis electrodynamic shaker Dongling ES-2-150. Digital-analogue-digital conversion of input and output signals was carried out at a sampling frequency of 200 Hz and the PSD calculation was performed with the resolution of 1024 spectral lines. The software and hardware tools used to drive the shaker and to acquire the test specimen response were from the LMS Test.Lab system. Piezoelectric accelerometers of PCB 353B03 and PCB 333B32 types were used to measure vertical accelerations on the shaker table near the cantilever clamp and on the mass at the free end of the specimen. Two more accelerometers to register vertical acceleration on the specimen close to the clamp and transversal acceleration of the mass (in order to detect possible excitation of torsional motion) are also present in Fig. 6 but the signals measured by them are not discussed in this paper.

To calculate FDS for the cantilever specimen described above, a SDOF system damping factor and a Wohler curve slope are required. These parameters were determined in preliminary experiments. Frequency response function (FRF) of the system under consideration was found by analyzing measurements of vibrations of the shaker table and the mass at the specimen free end. Since this specimen is treated as a SDOF system, the method of half-power points [20] was used for estimating the damping factor

$$\zeta = (\omega_2^2 - \omega_1^2)/(4\omega_p^2) \tag{10}$$

from three frequency values ω_p, ω_1, and ω_2 corresponding to positions of the resonance peak and two points on the FRF plot $F(\omega)$ where the mass amplitudes $F(\omega_1)$ and $F(\omega_2)$ squared become twice less than the peak amplitude $F(\omega_p)$ squared. Fifteen experimental runs of the FRF estimation with the subsequent calculation of ζ by Eq (10) were made and the average value of the damping factor ζ=2.8% was obtained from them.

To evaluate the Wohler curve slope b, a number of specimens were subjected to random excitations with the uniform PSD. Since accumulation of fatigue damage results in gradual decrease of the specimen resonance frequency, it can be assumed [21,22] that the specimen is not fatigue-resistant anymore (i.e. the fatigue failure occurs) when this frequency decrease reaches certain percentage of the initial resonance frequency. The times to failure defined by this criterion were registered for specimens tested at five different excitation RMS levels, with three specimens for each RMS value. Then, all points representing the experimental times to failure for corresponding RMS values were put on the logarithmic coordinate system and interpolated by a straight line of the estimated Wohler curve which appeared to have the slope b=5.8.

Both methods of random shaker testing with simultaneous PSD and kurtosis control discussed in Section 3 can be incorporated into an automatic closed-loop shaker controller but in this research a manual open-loop iterative procedure was set up in order to assess all intermediate results. On each iteration, a drive signal for the shaker amplifier input was prepared as a result of analysis of the shaker table acceleration feedback signal from the previous iteration. The PSD frequency lines and the kurtosis value were controlled according to Eqs (5) and (6). Experimental results obtained by the method of analytical phase selection based on the kurtosis equation are shown in Fig. 7 where the gray curve is the target PSD profile of car vibration recorded in typical operational conditions. The kurtosis value of this vibration was K=5.7.

a) 1st iteration: shaker vibration kurtosis $K_1^{vib} = 9.6$ was much higher than the target kurtosis $K_{spec} = 5.7$

b) 2nd iteration: shaker vibration kurtosis $K_2^{vib} = 5.2$ was lower than the target kurtosis $K_{spec} = 5.7$

c) 3rd iteration: shaker vibration kurtosis $K_3^{vib} = 6.3$ was higher than the target kurtosis $K_{spec} = 5.7$

d) 4th iteration: shaker vibration kurtosis K_4^{vib}=6.1 was slightly higher than the target kurtosis $K_{spec} = 5.7$

Fig. 7. PSDs of shaker vibration with kurtosis control by the analytical phase selection method (black curves) and the target PSD of car vibration recorded in operational conditions (gray curve)

On the first iteration (Fig. 7,a), the PSD of the shaker table vibration feedback signal (black curve) was essentially different from the target profile in the vicinity of the second peak (11.5 Hz) of the car vibration PSD, mildly different in the vicinity of the first PSD peak (7.7 Hz), and slightly different at the third PSD peak (15.3 Hz). The shaker vibration kurtosis value $K_1^{vib} = 9.6$ obtained on the first iteration was larger than the target kurtosis $K_{spec} = 5.7$ of the car vibration. It means that the drive signal kurtosis K_2^{dr} for the second iteration should be lower than it was on the first iteration and this K_2^{dr} value was calculated by Eq (6).

On the second iteration (Fig. 7,b) the comparison of the shaker vibration PSD and the car vibration PSD improved at the third peak to no difference and at the first peak to slight difference whereas at the second peak the difference was still essential because this peak coincided with the resonance frequency of the cantilever specimen mounted on the shaker table. When generating the drive signal for the second iteration, the shaker vibration kurtosis obtained on the first iteration needed to be decreased. This was achieved but the value of $K_2^{vib} = 5.2$ obtained was now smaller than the target kurtosis $K_{spec} = 5.7$.

On the third iteration (Fig. 7,c), the PSD simulation continued to improve with only a slight difference remaining between the shaker and car vibration PSDs in the vicinity of the second PSD peak with no difference at all other peaks. The kurtosis value $K_3^{vib} = 6.3$ appeared to be higher than $K_{spec} = 5.7$ by approximately the same amount for which it was smaller than the target on the previous iteration. This kurtosis difference was further decreased on the fourth iteration when $K_4^{vib} = 6.1$ value was obtained simultaneously with the shaker vibration PSD matching the car vibration PSD (see Fig. 7,d).

Thus, no further PSD corrections were needed and one more, the fifth, iteration, with the same drive signal PSD was carried out to refine the kurtosis value only. Consequently, the obtained shaker excitation kurtosis of $K_5^{vib} = 5.8$ provided a good match with the target kurtosis $K_{spec} = 5.7$. To complement the above results of the simultaneous PSD and kurtosis control experiment by the analytical phase selection method based on the kurtosis equation, time histories of all three kinds of the generated and measured signals (drive input, shaker vibration, and cantilever specimen response) will be shown and further discussed below.

6. Fatigue Damage Spectrum Calculations

When the shaker control procedure is finished and the generated shaker table vibration signal is recorded, FDS estimation can be done and its results compared for different methods of simulating environmental excitations. The FDS was calculated with the damping factor ζ=2.8% and the Wohler curve slope b=5.8 estimated as described in the previous section. In the research reported by this paper, the focus had been on one point of the FDS curve, with this point being the 12 Hz resonance frequency of the cantilever specimen mounted on the shaker. The FDS values obtained for all three methods of interest (Gaussian random, non-Gaussian with kurtosis by the time-frequency domain swapping, and non-Gaussian with kurtosis by the analytical phase selection method) were converted into time-to-failure (TTF) prediction determined as follows.

The FDS value obtained for one of possible resonance frequencies and for excitation of certain duration constitutes some fraction of the full damage for which the specimen would break according to prediction based on the Wohler curve. Since this full damage is expressed by unit value in the Miner rule, the inverse of the FDS value will indicate how many times the duration of the used excitation would need to be repeated until the specimen's breakage. This number of times multiplied by the duration of the excitation applied will be the estimated TTF for this excitation. The TTF values obtained for the aforementioned three excitation methods to be compared were finalized as values relative to the TTF predicted for the operational excitation from the car body vibration example under consideration.

The relative TTF results expressed in percentage form for the Gaussian and two kinds of non-Gaussian high-kurtosis excitations are presented in Table 1 alongside the experimental kurtosis values obtained for the shaker vibrations and specimen responses. These kurtosis values are certainly correlated to the resulting TTF values because the higher is the kurtosis of the specimen response, the more cycles with larger amplitudes are encountered in the stress time history and, consequently, the more severe damage is inflicted upon the unit under test. It can be seen from the first row of Table 1 that, if traditional Gaussian random testing was performed, it would be a significant undertesting because the resulting TTF appeared to be more than 6 times longer than the TTF predicted for the in-service road excitation.

Table 1 Results of shaker testing for car vibration with PSD specified in the interval from 5 to 45 Hz

	Random Control Methods	**Shaker vibration kurtosis**	**Specimen response kurtosis**	**TTF relative to road TTF**	**IFFT phase selection**
1	Traditional Gaussian random testing	3.0	3.0	630%	no phase manipulation, all phases are random
2	Time-frequency domain swapping to get shaker excitation kurtosis equal to that of car vibration on the road	5.8	3.4	570%	all phases are manipulated simultaneously
3	Time-frequency domain swapping to get maximum achievable shaker excitation kurtosis	6.5	4.2	450%	all phases are manipulated simultaneously
4	Analytical phase selection to get shaker excitation kurtosis equal to that of car vibration on the road	5.7	7.8	62%	phases from 8.3 to 14 Hz are manipulated but other phases remain random
5	Equivalent shaker testing by analytical phase selection to generate high-kurtosis excitation leading to TTF equal to TTF for the road excitation	4.0	6.9	100%	phases from 9.6 to 12.5 Hz are manipulated but other phases remain random
6	Accelerated shaker testing by analytical phase selection to generate high-kurtosis excitation leading to TTF less than the road excitation TTF	10.1	9.2	36%	phases from 5.8 to 13.4 Hz are manipulated but other phases remain random

Implementation of kurtosis control by the time-frequency domain swapping (the second row in Table 1) allowed to achieve slight improvement compared to the Gaussian excitation but the TTF obtained was still very big, 570% of the TTF for the road excitation. In an attempt to get better result, the target kurtosis value was made not the kurtosis of the road vibration but higher, as much as this method of kurtosis control could produce (see the third row in Table 1). In such a way the maximum achievable kurtosis appeared to be 6.5 and the resulting TTF estimation decreased to 450% that is, however, still much longer than the TTF for the road excitation.

When the method of polynomial transformation with time-frequency domain swapping was used, the kurtosis value of the specimen response appeared to be essentially lower than the corresponding kurtosis value of shaker vibration (see the second and third rows of Table 1). Because of the inability of this method to pass high kurtosis values from the generated shaker table vibration into the stress response of the unit under test, it was not possible to generate excitations with the estimated TTF short enough to match the TTF for the considered example of operational car vibration. Obviously, with the test specification of the equivalent qualification testing underachieved substantially, any kind of accelerated testing by the time-frequency domain swapping kurtosis increase becomes out of reach.

For the analytical phase selection based on the kurtosis equation the results were much more favorable. This method was capable of passing and even amplifying high kurtosis values from shaker vibration to

stress in the tested specimen (see the fourth, fifth, and sixth rows of Table 1). The relative TTF estimated in the case of shaker excitation kurtosis equal to that of car vibration on the road was 62% (the fourth row in Table 1). Obviously, it is over-testing with the shaker vibration of the same kurtosis as in operation but inflicting more damage than the operational car vibration. Therefore, further action was taken to make the shaker excitation less damaging and to bring the corresponding TTF to the TTF estimated for the road excitation.

Two more shaker control iterations were performed with the drive signal PSD unchanged and the kurtosis value decreasing. The result is presented in the fifth row of Table 1. When the shaker vibration kurtosis was reduced to 4, the response kurtosis of the cantilever specimen dropped from 7.8 to 6.9, and the TTF value has become equal to the on-road TTF. That is what was necessary for equivalent testing, just to simulate operational excitations in the laboratory. To achieve accelerated testing with TTF less than the TTF for the road excitation, one needs to return to control iterations and now select IFFT phases in such a way that kurtosis of drive signals is increasing. Distinct from the polynomial transformation with time-frequency domain swapping, the analytical phase selection method has potential of doing so.

The last row of Table 1 contains results of accelerated testing achieved by the analytical phase selection method based on the kurtosis equation. More phases were involved in the phase manipulation process and much higher kurtosis value of the drive signal was produced to increase the shaker vibration kurtosis from K=5.7 (as for the road excitation) to K=10.1. As a result, the shaker excitation was made more severe than the road excitation and accelerated testing has become possible. The cantilever specimen response kurtosis increased from K=6.9 to K=9.2 and time histories of all three signals involved can be seen in Fig. 8.

a) Input drive signal (K=19) b) Shaker table vibration (K=10.1) c) Specimen response (K=9.2)

Fig. 8. Excitation and response signals in accelerated testing by the analytical phase selection method with the TTF for shaker excitation estimated to be 36% of the TTF for road excitation.

The above results and their discussion demonstrate that the analytical phase selection method based on the kurtosis equation is capable of controlling the FDS. Various TTF values were achieved, ranging from an equivalent TTF (the same as for operational vehicle vibration) to a TTF enabling an accelerated lifetime test with the acceleration factors up to three times compared to equivalent testing. However, in this experiment the FDS control was carried for one frequency point (12 Hz) whereas normally the FDS assessment is a curve drawn over the certain frequency interval. Therefore, it was of interest to see whether accelerated testing was also achieved for other frequency points of the conventional FDS plot.

The FDS curve shown in Fig. 9 was calculated for the frequency interval from 5.8 to 13.4 Hz where the IFFT phases of the input drive signal were manipulated by the analytical phase selection method to achieve the aforementioned relative TTF of 36% at the frequency of 12 Hz. As can be seen in Fig. 9, accelerated testing was also ensured for most of other frequencies in the considered interval. However, in the vicinity of 8 Hz, the estimated relative TTF for this shaker excitation appears to be more than 100%, i.e. the test TTF was longer than the TTF for the road excitation. Hence, it would be useful to develop a method of reshaping the FDS and TTF curves by controlling their values not at just one but at several frequency points simultaneously.

Fig. 9. TTF for accelerated testing relative to TTF for the road excitation

7. Discussion

The kurtosis control methods were initially introduced into shaker testing practice for more accurate simulation of operational vibrations experienced by components and passengers of land vehicles but now the same approach is considered for another purpose of deliberately increasing severity of shaker

excitations in order to carry out fatigue durability testing in a shorter time. Kurtosis increase means presence of higher peaks in the random signal time history and, if such an effect occurs for stress response in the unit under test then more cycles with high amplitude will inflict more fatigue damage that is required for accelerated testing.

For shaker control systems based on the IFFT procedure, an effective approach for matching both the specified PSD and kurtosis is to arrange signal variables such that the amplitudes are responsible for the PSD as usual but some of the phases are now used to adjust kurtosis instead of all of them being random as in the traditional IFFT signal generation. The PSD and kurtosis corrections can be done simultaneously in the same iteration process of the shaker controller setup. Possible methods of phase manipulation are presented above and discussed in relation to the specifics and requirements of in-house qualification testing of vehicle components with the use of the fatigue damage spectrum model.

The first method of polynomial transformation with time-frequency domain swapping is an iterative procedure to operate with all phases starting from their random values towards those phases that provide the required kurtosis value. The second method is an analytical solution of purposely selecting some phases while leaving the rest of them random. It is based on the closed-form expression of kurtosis via the amplitudes and phases of the IFFT-generated signal. Previously both these methods were used in the case of the unit under test being fixed to the shaker table rigidly. However, it is different with the fatigue damage spectrum model considered in this paper because the unit under test is supposed to be a SDOF system with its elastic element being prone to fatigue failure.

The problem is that the response of a lightly-damped linear SDOF system assumed by the FDS model becomes closer to a Gaussian random signal than the applied non-Gaussian excitation signal. Even if the shaker table vibration possesses high kurtosis, this excitation signal may be of inappropriate nature to achieve higher enough kurtosis for the stress response signal of the SDOF elastic element. As the numerical and experimental results suggest, the method of analytical phase selection based on the kurtosis equation is capable of passing high kurtosis values from shaker vibration to stress in the tested specimen and making accelerated testing feasible.

On the other hand, by the method of polynomial transformation with time-frequency domain swapping, it was not possible to achieve the stress response kurtosis necessary for accelerated testing and even to subject the tested specimen to the same severity as that of the in-service car vibration. However, this method may still be useful in auxiliary role of being added to the method of analytical phase selection in order to have background vibration between the main high peaks in the stress response more variable than it is when the analytical phase selection is implemented on its own.

8. Conclusions

Two methods of generating random vibrations with increased kurtosis were considered in relation to the specifics and requirements of fatigue durability testing of vehicle components on electrodynamic shakers. It was demonstrated numerically and verified experimentally that, with the use of kurtosis control by analytical selection of IFFT phases based on the closed-form kurtosis equation, the accelerated testing can be carried out without any increase of the excitation level thereby avoiding caveats inherent to methodologies of scaling up the PSD corresponding to in-service conditions.

A real example of car body vibration measured in operation was simulated for shaker testing of cantilever specimens and subsequent evaluation of fatigue damage accumulated as a result of random excitation in the vicinity of the specimen's resonance. Various estimated time-to-failure values were achieved by changing the shaker excitation kurtosis. Starting from the time-to-failure equivalent to the effect of operational vibration, shorter time-to-failure values were possible up to the acceleration factor equal to three.

Acknowledgement

This research was supported by the Marie Curie International Incoming Fellowship (Project N° 328961 "RANGE") within the 7th European Community Framework Programme.

References

[1] Test Method Standard MIL-STD-810G. Environmental Engineering Considerations and Laboratory Tests, *US Department of Defense*, 2008.

[2] Lee, Y.-L. and Kang, H.-T., "Vibration Fatigue Testing and Analysis," *Metal Fatigue Analysis Handbook: Practical Problem-Solving Techniques for Computer-Aided Engineering*, Y.-L. Lee, M.E. Barkey, H.-T. Kang, Eds., Butterworth-Heinemann/Elsevier, Waltham, MA, USA, 2011.

[3] Lalanne, C., *Mechanical Vibration and Shock Analysis – Volume 5: Specification Development*, 3rd edition, John Wiley & Sons, London, 2014.

[4] Piersol, A. G., "Accelerated Vibration Testing - Proceed with Caution," *Tustin Training News,* 1993.

[5] Hieber, G. M., "Use and Abuse of Test Time Exaggeration Factors," *TEST Engineering and Management*, Apr/May, 1999, pp. 14-16.

[6] Connon, W. H., "Comments on Kurtosis of Military Vehicle Vibration Data," *Journal of the Institute of Environmental Sciences*, No 6, 1991, pp. 38-41.

[7] Steinwolf, A., "Shaker Simulation of Random Vibrations with a High Kurtosis Value," *Journal of the Institute of Environmental Sciences*, No 3, 1997, pp. 33-43.

[8] Smallwood, D. O., "Generating Non-Gaussian Vibration for Testing Purposes," *Sound and Vibration*, Vol. 39, No 10, 2005, pp. 18-24.

[9] Van Baren, P. D., "System and Method for Simultaneously Controlling Spectrum and Kurtosis of a Random Vibration," *US Patent No.* 7,426,426, 2008.

[10] Steinwolf, A., "Random Vibration Testing with Kurtosis Control by IFFT Phase Manipulation," *Mechanical Systems and Signal Processing*, Vol. 28, 2012, pp. 561-573.

[11] Steinwolf, A. "Vibration Testing by Non-Gaussian Random Excitations with Specified Kurtosis. Part I Discussion and Methods," *Journal of Testing and Evaluation*, Vol. 42, No. 3, 2014, pp 659-671.

[12] Van Baren, J. and Van Baren, P., "The Fatigue Damage Spectrum and Kurtosis Control," *Sound and Vibration*, Vol. 46, No 10, 2012, pp. 10-13.

[13] Kihm, F., Rizzi, S. A., Ferguson, N. S., and Halfpenny, A., "Understanding How Kurtosis Is Transferred from Input Acceleration to Stress Response and Its Influence on Fatigue Life", *Proceedings of the 8th International Conference on Recent Advances in Structural Dynamics*, Pisa, Italy, July 1-3, 2013.

[14] Troncossi, M. and Rivola, A., "Response Analysis of Specimens Excited with Non-Gaussian Acceleration Profiles", *Proceedings of the 11th International Conference on Noise and Vibration Engineering - ISMA2014*, Leuven, Belgium, September 15-17, 2014, pp. 799-808.

[15] Winterstein, S. R., "Nonlinear Vibration Models for Extremes and Fatigue," *ASCE Journal of Engineering Mechanics*, Vol. 114, 1988, pp. 1772-1790.

[16] Steinwolf, A., "Vibration Testing by Non-Gaussian Random Excitations with Specified Kurtosis. Part II: Numerical and Experimental Results," *Journal of Testing and Evaluation*, Vol. 42, No. 3, 2014, pp 672-686.

[17] Van der Ouderaa, E., Schoukens, J., and Renneboog, J., Peak Factor Minimization Using a Time-Frequency Domain Swapping Algorithm," *IEEE Transactions on Instrumentation and Measurement*, Vol. 37, No 1, 1988, pp. 145–147.

[18] Carrella, A. and Peeters, B., "Using Kurtosis Control with Random-Control Vibration Tests," *Proceedings of the 26th International Conference on Noise and Vibration Engineering*, ISMA 2014, Leuven, Belgium, September 15-17, 2014, pp. 715-722.

[19] Steinwolf, A., "Approximation and Simulation of Probability Distributions with a Variable Kurtosis Value," *Computational Statistics and Data Analysis*, Vol. 21, No. 2, 1996, pp. 163–180.

[20] Ewins, D.J., *Modal Testing: Theory, Practice and Applications*, Research Studies Press, 2000.

[21] Khalij, L., Gautrelet, C., and Guillet, A., "Fatigue Curves of a Low Carbon Steel Obtained from Vibration Experiments with an Electrodynamic Shaker", *Materials and Design*, Vol. 86, 2015, pp. 640–648.

[22] Angeli, A., Cornelis, B., and Troncossi, M., "Synthesis of Sine-on-Random vibration profiles for accelerated life tests based on Fatigue Damage Spectrum equivalence", *Mechanical Systems and Signal Processing*, Vol. 103, 2018, pp. 340-351.

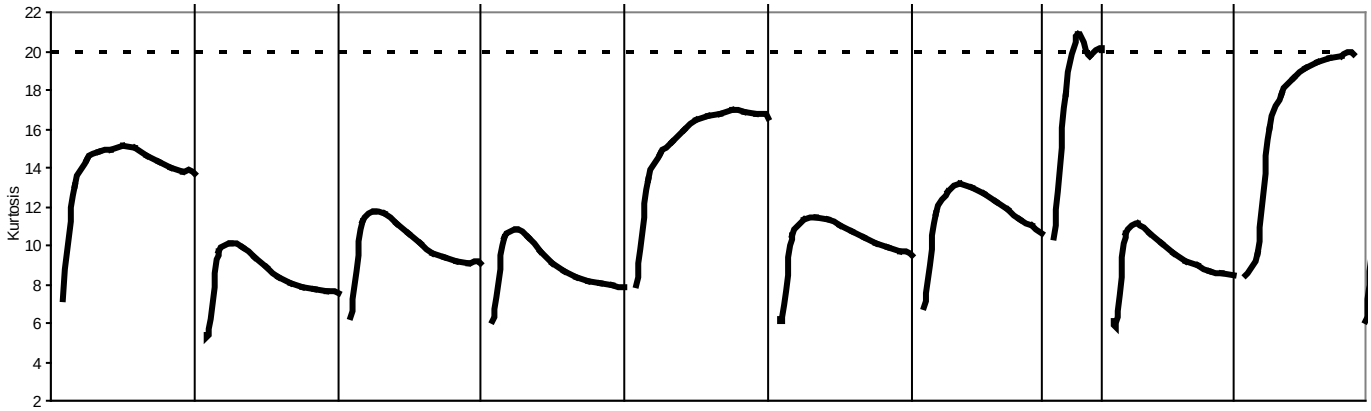

a) Kurtosis results for wideband PSD profile with 1000 frequency lines

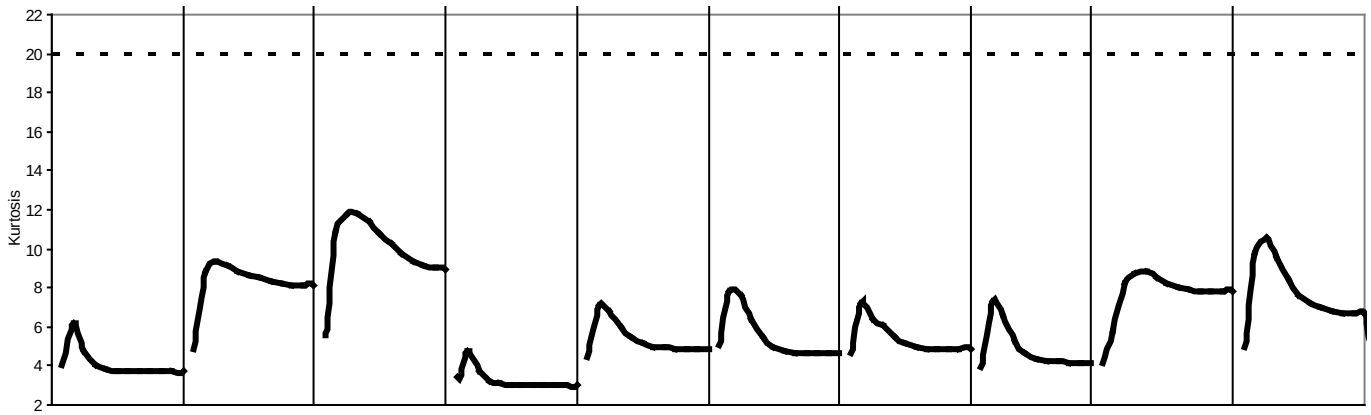

b) Kurtosis results for narrowband PSD profile with 100 frequency lines

Fig. 1. Time-frequency domain swapping iteration processes demonstrating maximum kurtosis values achieved for different IFFT data blocks

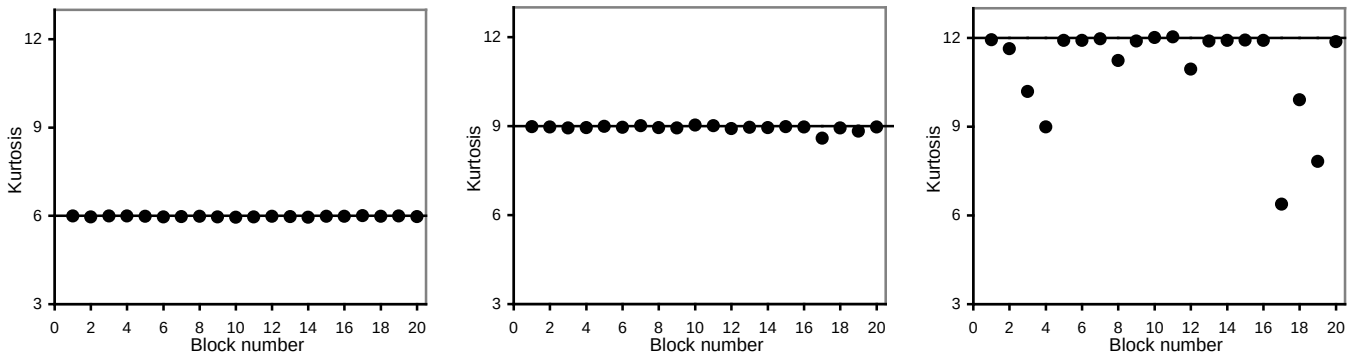

a) K=6 in 100% of blocks, K_t=6 b) K=9 in 95% of blocks, K_t=8.9 c) K=12 in 60% of blocks, K_t=11

Fig. 2. Kurtosis simulation success rates by the method of polynomial transformation with time-frequency domain swapping for PSD profile with 1000 frequency lines.

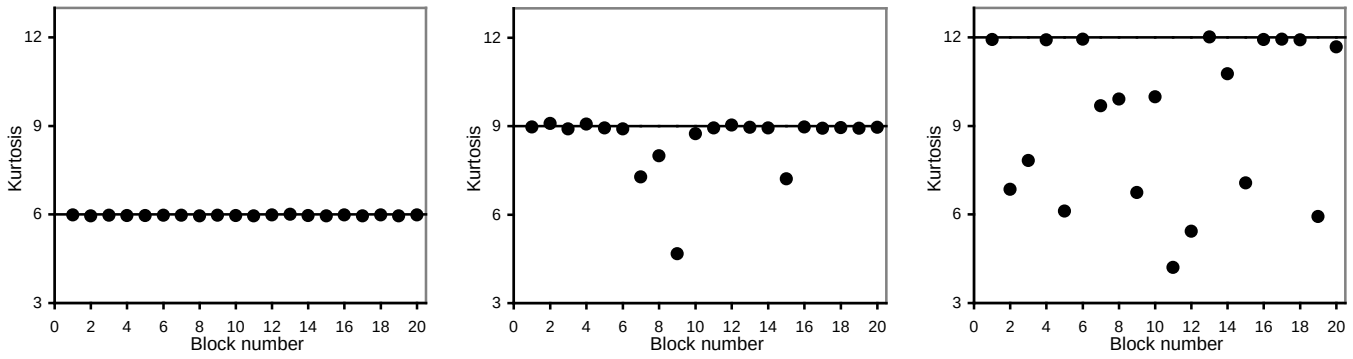

a) K=6 in 100% of blocks, K_t=6 b) K=9 in 75% of blocks, K_t=8.5 c) K=12 in 35% of blocks, K_t=9.4

Fig. 3. Kurtosis simulation success rates by the method of polynomial transformation with time-frequency domain swapping for PSD profile with 500 frequency lines.

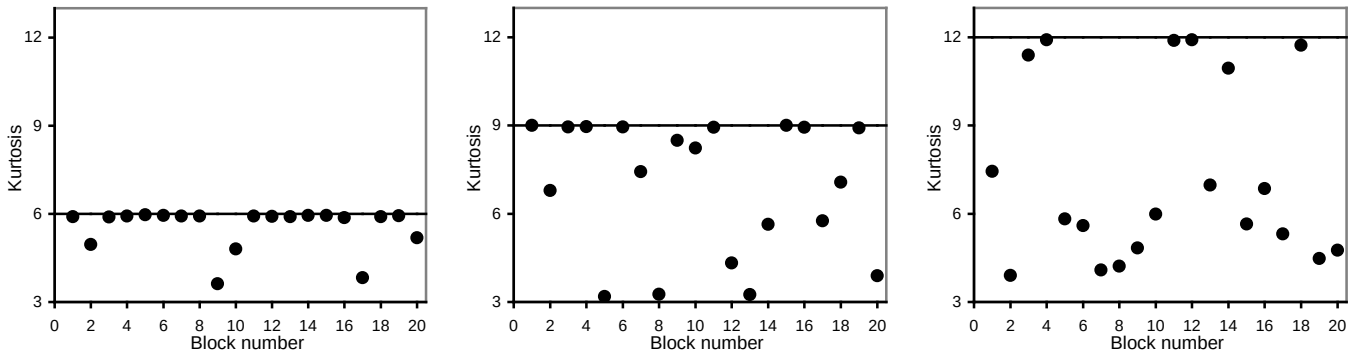

a) K=6 in 75% of blocks, K_t=5.6 b) K=9 in 40% of blocks, K_t=6.9 c) K=12 in 15% of blocks, K_t=7.3

Fig. 4. Kurtosis simulation success rates by the method of polynomial transformation with time-frequency domain swapping for PSD profile with 100 frequency lines.

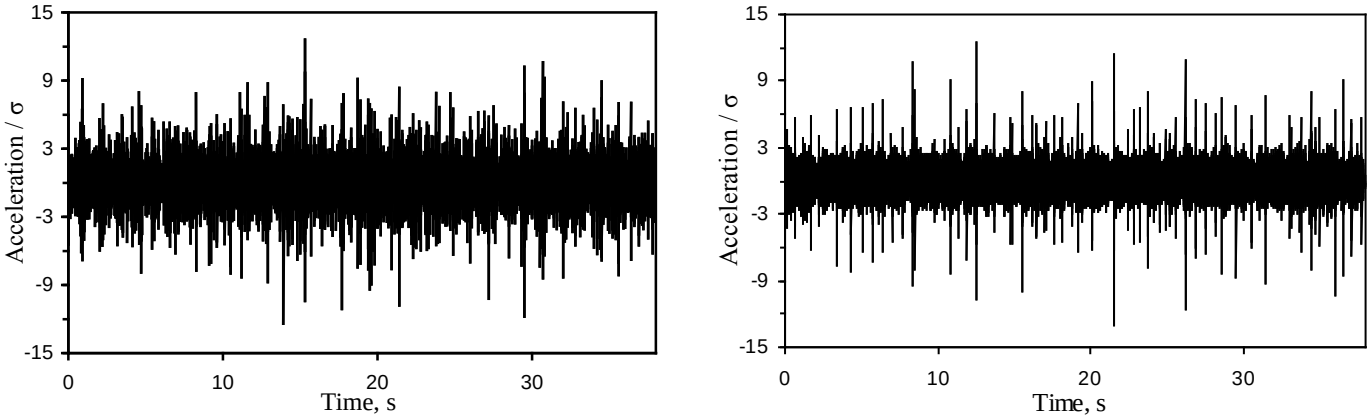

a) Polynomial transformation with time-frequency domain swapping

b) Analytical phase selection based on kurtosis equation

Fig. 5. Shaker excitation time histories generated by two different methods of kurtosis control.

Fig. 6. Experimental setup: the cantilever specimen mounted on the shaker.

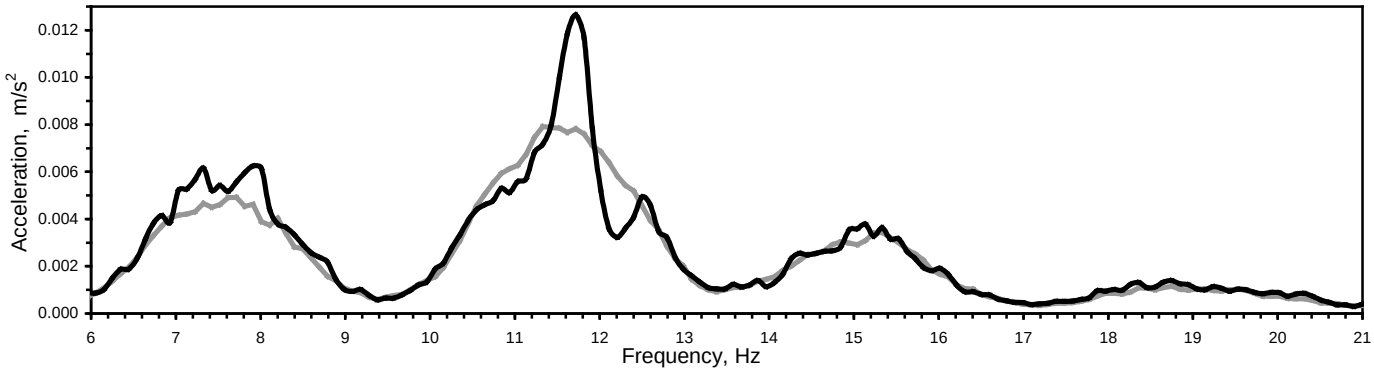

a) 1st iteration: shaker vibration kurtosis $K_1^{vib} = 9.6$ was much higher than the target kurtosis $K_{spec} = 5.7$

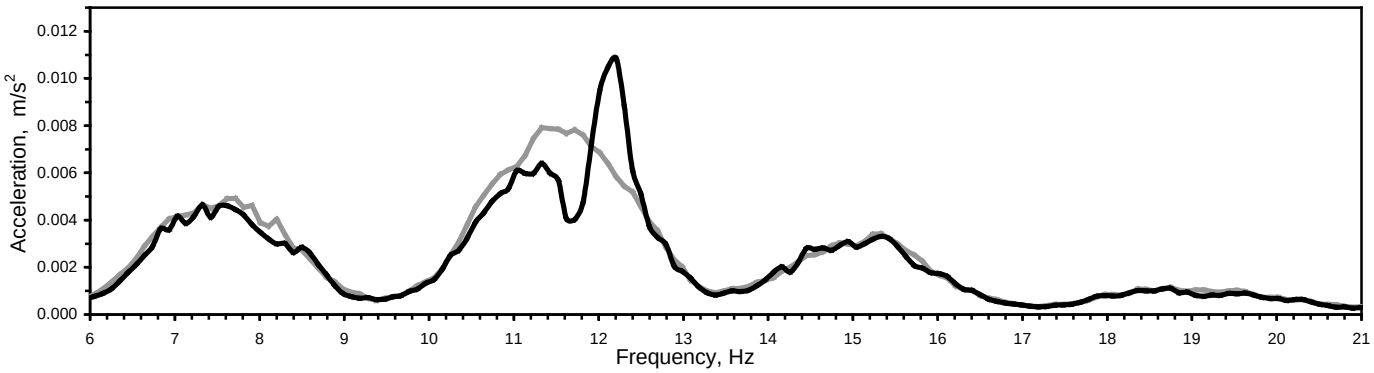

b) 2nd iteration: shaker vibration kurtosis $K_2^{vib} = 5.2$ was lower than the target kurtosis $K_{spec} = 5.7$

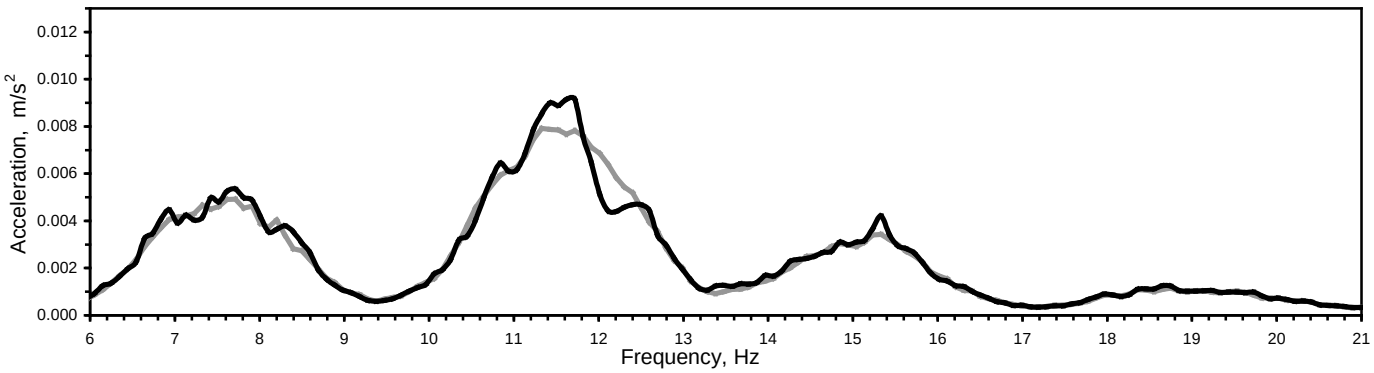

c) 3rd iteration: shaker vibration kurtosis $K_3^{vib} = 6.3$ was higher than the target kurtosis $K_{spec} = 5.7$

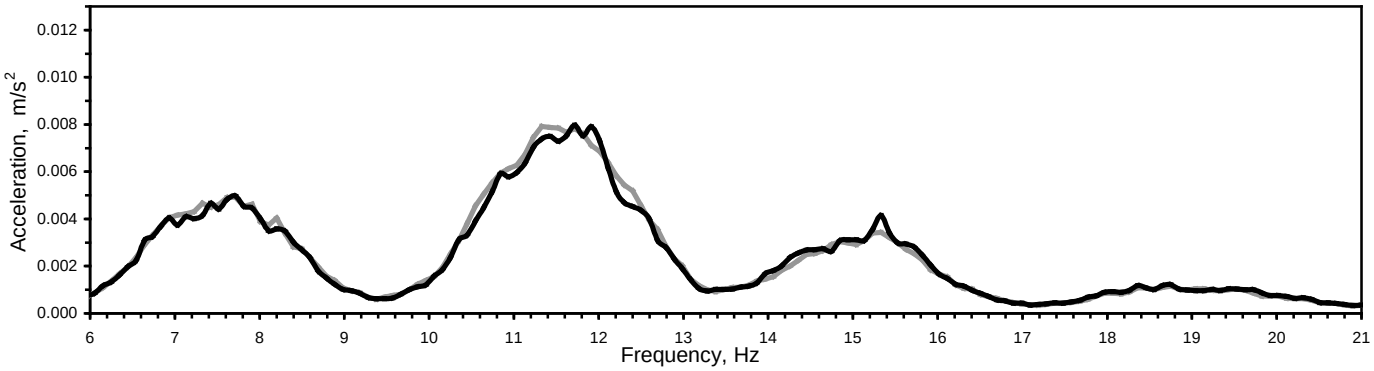

d) 4th iteration: shaker vibration kurtosis K_4^{vib}=6.1, just slightly higher than the target kurtosis $K_{spec} = 5.7$

Fig. 7. PSDs of shaker vibration with kurtosis control by the analytical phase selection method (black curves) and the target PSD of car vibration recorded in operational conditions (gray curve)

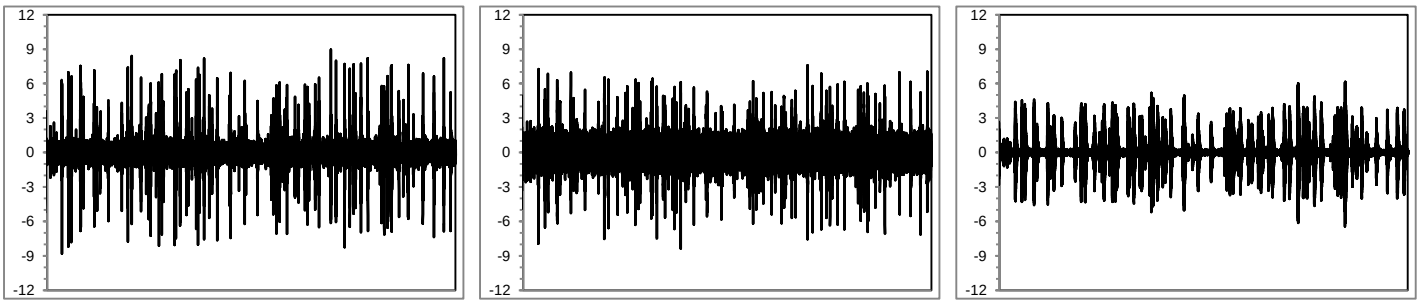

a) Input drive signal (K=19) b) Shaker table vibration (K=10.1) c) Specimen response (K=9.2)

Fig. 8. Excitation and response signals in accelerated testing by the analytical phase selection method with the TTF for shaker excitation estimated to be 36% of the TTF for road excitation.

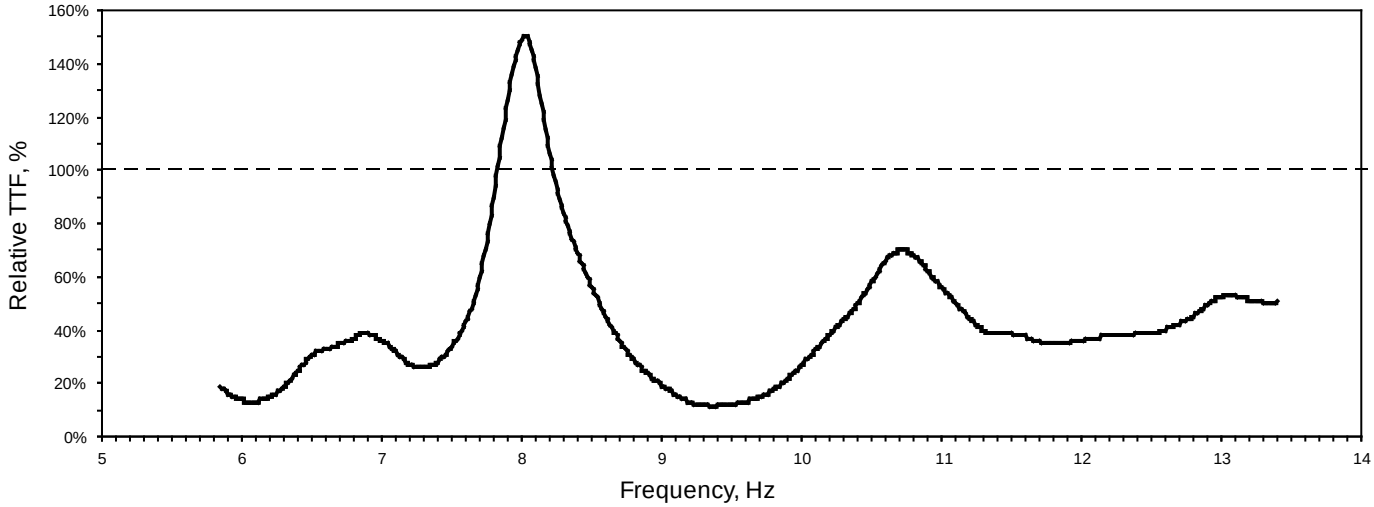

Fig. 9. TTF for accelerated testing relative to TTF for the road excitation